


Cite this: DOI: 10.1039/d0dt00958j

# Role of size, alio-/multi-valency and non-stoichiometry in the synthesis of phase-pure high entropy oxide (Co,Cu,Mg,Na,Ni,Zn)O<sup>†</sup>

Nandhini J. Usharani,<sup>a</sup> Rajat Shringi,<sup>a</sup> Harshil Sanghavi,<sup>a</sup> S. Subramanian<sup>b</sup> and S. S. Bhattacharya  <sup>\*a</sup>

A nanocrystalline high entropy oxide with near-equi-molar composition consisting of 5 transition metal cations and one alkali cation (Co,Cu,Mg,Na,Ni,Zn)O was synthesised by a reverse co-precipitation (RCP) process and characterised by standard methods of X-ray diffraction (for crystallite size and phases), electron microscopy (for particle morphology and size distribution) and Fourier transform *infra*-red spectroscopy (for bond identification and bond lengths). Charge compensation in the lattice by the formation of Co<sup>3+</sup> and/or Ni<sup>3+</sup> (in order to offset the +1 oxidation state of Na) and the creation of oxygen vacancies was quantified from X-ray photoelectron spectroscopy and Raman spectroscopy and further studied using vibrating sample magnetometry (VSM). The influence of different transition metals in being able to accommodate the larger and aliovalent sodium ion in a single phase-pure rocksalt lattice was investigated and the criteria for element selection in such multicomponent systems for single-phase formation examined. Presence of multivalency/non-stoichiometry to accommodate a different-sized cation and maintaining electroneutrality were identified as the critical criteria for single-phase formation in multicomponent systems and further confirmed through synthesis of various lower combination systems (by systematic removal of one transition metal cation) and by addition of bivalent Ca as well as cations of higher valencies. These criteria would aid in designing the compositions of high entropy oxides with aliovalent substitutions.

Received 13th March 2020,

Accepted 3rd May 2020

DOI: 10.1039/d0dt00958j

rsc.li/dalton

## 1 Introduction

The quest for new materials with improved and novel properties has always been the greatest motivation for the development of different classes of materials that include equimolar or near-equimolar multicomponent systems. The precursor for such systems were the high entropy alloys, where five or more elements could be substituted into a single lattice to form solid solutions.<sup>1</sup> The basic criteria for the selection of these elements were based on Hume-Rothery and Pauling's rules, which include nearby ionic radii, same co-ordination number for a specific lattice structure and same oxidation state. Using these criteria,

Rost *et al.*<sup>2</sup> were the first to synthesise a phase-pure (Co,Cu,Mg,Ni,Zn)O system with a rocksalt structure, opening up the field of "high entropy oxides". In their work at least one cation was chosen such that it did not form a complete isomorphous solid solution and ensured that it was not just isovalent substitution and the involvement of high configurational entropy in stabilizing the structure was demonstrated. Following this pioneering effort other systems such as (Ce<sub>0.2</sub>La<sub>0.2</sub>Pr<sub>0.2</sub>Sm<sub>0.2</sub>Y<sub>0.2</sub>)O<sub>2-δ</sub><sup>3</sup> and (Zr<sub>0.2</sub>Sn<sub>0.2</sub>Ti<sub>0.2</sub>Hf<sub>0.2</sub>Ce<sub>0.2</sub>)O with fluorite structure,<sup>4</sup> (Gd<sub>0.2</sub>La<sub>0.2</sub>Nd<sub>0.2</sub>Sm<sub>0.2</sub>Y<sub>0.2</sub>)(Co<sub>0.2</sub>Cr<sub>0.2</sub>Fe<sub>0.2</sub>Mn<sub>0.2</sub>Ni<sub>0.2</sub>)O<sub>3</sub> and (Sr<sub>0.2</sub>Ba<sub>0.2</sub>)(Zr<sub>0.2</sub>Sn<sub>0.2</sub>Ti<sub>0.2</sub>Hf<sub>0.2</sub>Nb<sub>0.2</sub>)O<sub>3</sub> with perovskite structure<sup>5,6</sup> and (Co,Cr,Fe,Mn,Ni)<sub>3</sub>O<sub>4</sub> with spinel structure have been synthesized.<sup>7</sup> However, in all the cases the criteria behind the selection of the cations have, more or less, remained the same, with particular emphasis being placed on the cations having the same stable oxidation state as well as similar sizes. The use of an aliovalent cation with a totally different stable oxidation state and a considerably different size in forming a single-phase structure in such equimolar multicomponent systems is yet to be fully explored. In general, aliovalent cationic substitutions in unary or binary oxides have been done to a limited quantity of the aliovalent cation (such as doping) in order to obtain an

<sup>a</sup>Nano Functional Materials Technology centre, (NFMTC), Department of Metallurgical and Materials engineering, Indian Institute of Technology Madras, Chennai-600036, India. E-mail: ssb@iitm.ac.in; Tel: +91 94447 78122

<sup>b</sup>Sophisticated Analytical Instrument Facility, Indian Institute of Technology Madras, Chennai-600036, India

<sup>†</sup>Electronic supplementary information (ESI) available: Rietveld refinement pattern of (Ca,Co,Cu,Mg,Ni,Zn)O, (Cu,Mg,Na,Zn)O, *d*-spacing and *hkl* planes of (Co,Cu,Mg,Ni,Na,Zn)O, Composition from EDS, Binding energy from XPS for each cation and the literature used for assignment and Ionic radii difference of each cation as compared to Ni<sup>2+</sup>. See DOI: 10.1039/d0dt00958j

improvement in the properties of the respective unary or binary oxide.

Sodium has been doped in transition metal oxides such as NiO, or CoO for thermoelectric applications, as it improves the electrical conductivity and efficiency of the thermoelectric material.<sup>8,9</sup> Often a layered structure is formed when sodium is added to transition metal oxides, and used for battery applications.<sup>10</sup> Bérardan *et al.*,<sup>11</sup> have carried out monovalent ion doping such as Li and Na in a microcrystalline high entropy (Co,Cu,Mg,Ni,Zn)O oxide and observed high room temperature ionic conductivities of  $8 \times 10^{-6}$  and  $6 \times 10^{-6}$  S cm<sup>-1</sup> respectively for the Li and Na doped systems. High ionic conductivity in such Na doped systems could find potential applications as electrolytes in Na ion batteries, which are being considered as future candidates for replacing the more expensive Li ion batteries.<sup>12</sup> In general, materials show increased ionic conductivity in the nanocrystalline form due to the larger proportion of grain boundaries.<sup>13,14</sup> Sarkar *et al.*<sup>15</sup> have reported the synthesis of entropy stabilized (Co,Cu,Mg,Ni,Zn)O system in the nanocrystalline form and it has been shown that (Co,Cu,Mg,Ni,Zn)O can be used as a cathode in Li-ion batteries<sup>5</sup> with a stability of more than 500 cycles while retaining the capacity. Recent studies have also demonstrated the potential of such a high entropy oxide as anode material for Li-ion batteries.<sup>16</sup> In this study nanocrystalline (Co,Cu,Mg,Na,Ni,Zn)O, termed Na-TMO, was synthesised by a reverse co-precipitation process and the “stable oxidation state” criterion used for cation selection for the formation of a phase-pure rock salt lattice examined. For the sake of comparison and improved understanding a pure transition metal oxide based (Co,Cu,Mg,Ni,Zn)O system, termed ME-TMO as well as the (Co,Cu,Mg,Na,Ni,Zn)O system with one transition metal cation being systematically removed in order to determine the influence of the particular cation in stabilizing the structure were also synthesized.

## 2 Experimental details

Nickel(II) nitrate hexahydrate (99%, Alfa Aesar), cobalt(II) nitrate hexahydrate (99%, Alfa Aesar), magnesium nitrate hexahydrate (99%, Alfa Aesar), copper nitrate pentahydrate (99%, Alfa Aesar), zinc nitrate hexahydrate (99%, Alfa Aesar), calcium nitrate tetrahydrate (99%, Alfa Aesar), potassium nitrate (99%, Alfa Aesar), chromium nitrate nonahydrate (98.5%, Alfa Aesar), manganese nitrate hexahydrate, (98%, Alfa Aesar), iron nitrate nonahydrate (98%, Alfa Aesar) and sodium nitrate (99%, Alfa Aesar) were used as the individual precursors for the metal cations. The requisite quantity of the metal nitrates (as per the stoichiometric requirement for equimolar concentration) was dissolved in deionised water to form a final precursor of 1 M concentration. The precursor solution was added dropwise to ammonia solution (25%, Merck) in an ultrasonicated water bath with the pH being maintained between 10.5 and 11. The high pH of the solution ensured that precipitation of all the cations occurred simultaneously thereby enhancing the formation of a single phase. The precipitate consisting of a hydroxylated complex of the

metal cations was dried in an air oven at 120 °C. The dried precipitate was then calcined in a furnace at 1000 °C for two hours to form the multicomponent oxide.

## 3 Characterisation

Identification of the phases and analysis of the phase composition and crystallite size of the synthesized powders was carried out using an X-ray diffractometer (Panalytical) in the 2θ range of 10–90°, at a step size of 0.02°/2θ s. with Cu Kα radiation (1.5406 Å). Rietveld refinement was done using the Fullprof software suite® with a pseudo-Voigt model. The parameters refined were scale factor, zero shift, background, lattice parameters, FWHM parameters, shape parameter and oxygen occupancy. Magnetic measurement was carried out with by vibrating sample magnetometry (Lakeshore VSM 7410) at room temperature from –1.5 T to 1.5 T. The particle sizes and morphology were determined using a scanning electron microscope (FEI, Quanta 400) operating at 20 kV and a transmission electron microscope (FEI, Technai 20G<sup>2</sup>) operating at 200 kV. Bond identification and analysis was done using a Fourier transform infrared spectrometer (PerkinElmer, Spectrum 1) in the range of 400 cm<sup>-1</sup> to 3500 cm<sup>-1</sup>. Raman analysis was carried out by confocal Raman spectroscopy (WITec alpha 300) equipped with an Nd:YAG laser (532 nm) as the excitation source. X-ray photoelectron spectroscopy studies was done using a SPECS instrument with Al-Kα as the X-ray source and PHOIBOS 100MCD as the analyzer under ultrahigh vacuum (10<sup>-10</sup> mbar). The spectra were calibrated for charging by fixing the carbon peak at 284.8 eV. Quantification of the oxidation states of the cations has been carried out on the inner shell 2p orbital for all the cations except sodium, where the 1s orbital was used.

## 4 Results and discussion

### 4.1 Structure analysis through XRD and correlation with magnetic behaviour

XRD pattern of the (Co,Cu,Mg,Na,Ni,Zn)O system (Fig. 1(a)) revealed a phase-pure product with rocksalt crystal structure in

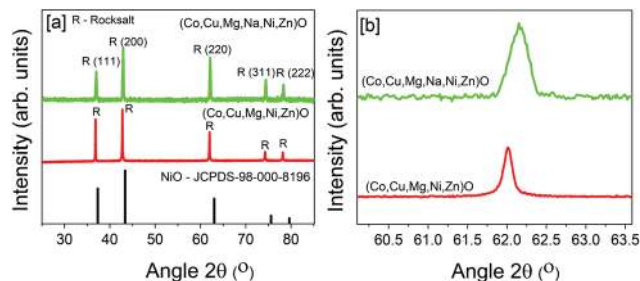


Fig. 1 (a) X-ray diffraction patterns of ME-TMO and Na-TMO (b) (220) XRD peaks of ME-TMO and Na-TMO, show the decreased lattice parameter (from the right shift of the Na-TMO peak) and increased peak broadening of Na-TMO shows decreased crystallite size.

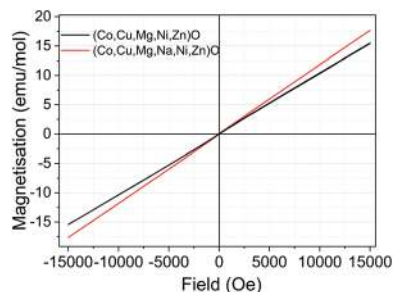


Fig. 2  $M$ - $H$  characteristics of ME-TMO and Na-TMO at room temperature.

the space group of  $fm\bar{3}m$ . The observed minor asymmetries present in the X-ray diffraction peaks (Fig. 1(b)) were attributed to distortions in the lattice. Similar observations have been reported in the case of NiO below the Néel temperature where the structure is either a distorted rock salt or monoclinic in nature and was accounted for in terms of exchange-striction causing a change in the lattice parameter and symmetry in order to reduce the exchange interaction energy.<sup>17</sup> The  $M$ - $H$  characteristics of the Na-TMO and ME-TMO systems are shown in Fig. 2 where it is seen that the magnetisation of Na-TMO is higher compared to the ME-TMO system, implying a higher  $J$  interaction (as  $J$  is directly proportional to the magnetisation).<sup>18</sup> Space group of the distorted structure was analysed to be monoclinic with the space group of  $(C\ 1\ 2/m\ 1)$ . Rietveld refinement was carried out with the monoclinic structure and the cell volume of Na-TMO was found to be 0.22% higher compared to the ideal cubic structure, while that of the ME-TMO was only 0.10% higher. This showed that the distortion was higher in the Na-TMO indicating greater exchange-striction in the system when compared to the ME-TMO. Lattice parameters of both the compositions in the distorted rocksalt (monoclinic) form are listed in Table 1 and it can be seen that the lattice parameter of Na-TMO (ideal cubic lattice) is lesser than that of the ME-TMO (and explained in detail in section 4.7). The Rietveld refined patterns are shown in Fig. 3(a) and (b).

#### 4.2 Crystallite size analysis through XRD

The crystallite sizes for the Na-TMO and ME-TMO systems were calculated using the Scherrer formula. It was seen that the crystallite size of the Na-TMO (30 nm) was less than that of the ME-TMO (81 nm). Such a decrease in the crystallite size on doping or alloying with a heterostructure cation has been reported earlier<sup>19</sup> and can be explained in the terms of the

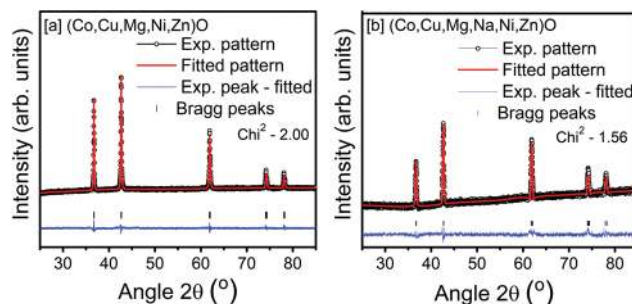


Fig. 3 (a) Rietveld refinement of ME-TMO (b) Rietveld refinement of Na-TMO, ( $hkl$  plane and  $d$ -spacing and 2-theta angle of the refined pattern is given in the Table S1† and occupancy of the cations are given in Table S2†).

growth mechanism. Typically, oxide formation during synthesis has two stages: homogeneous nucleation of monomers with critical size, followed by polynuclear growth. During the growth process ions diffuse into the nuclei to form a solid solution and for this diffusion to take place the ion has to bind itself to the nuclei for a specific residence time which depends on the binding energy.<sup>20</sup> In case of atoms/oxides of the same type, the binding energy of the atoms would be nearly uniform and the residence time required for diffusion would be less. On the other hand, as the larger, aliovalent Na has an antifluorite parent lattice in the oxide form, it can be expected that Na would require a higher residence time for diffusion into the nuclei. This would hinder the growth of the nuclei causing the number of nuclei being produced higher compared to the growth, thereby resulting in a lower crystallite size of the product compared to ME-TMO. Further, with  $\text{Na}^{1+}$  would require only a single electron transfer for an octet electronic configuration and so, bond termination would take place easily when Na ion is present, resulting in a smaller crystallite size.

#### 4.3 Electron microscopy analysis

SEM observations revealed that the particles of Na-TMO had formed agglomerates of polyhedra, but the actual morphology could not be discerned. On the other hand, in case of the ME-TMO particles no defined shape could be discerned as irregular hollow flakes with a lower degree of agglomeration were observed. Since sodium has high electron affinity, it could have increased the surface charge and hence, resulted in the particles being more agglomerated when compared to ME-TMO. The SEM micrographs of Na-TMO and ME-TMO are shown in Fig. 4. The composition, analysed by energy disper-

Table 1 Rietveld refinement parameters of cubic and monoclinic (distorted rocksalt) structure and other parameters obtained from X-ray diffraction data

Composition	Cubic		Monoclinic lattice parameters						Crystallite size (nm)	Strain (%)
	$a$ (Å)	$\chi^2$	$a$ (Å)	$b$ (Å)	$c$ (Å)	$\beta$ (°)	Volume (Å <sup>3</sup> )	$\chi^2$		
Na-TMO	4.235	1.56	5.198	2.998	2.990	125.273	38.063	1.52	30	0.09
ME-TMO	4.237	1.66	5.191	2.993	2.996	125.206	38.070	2.00	81	0.01



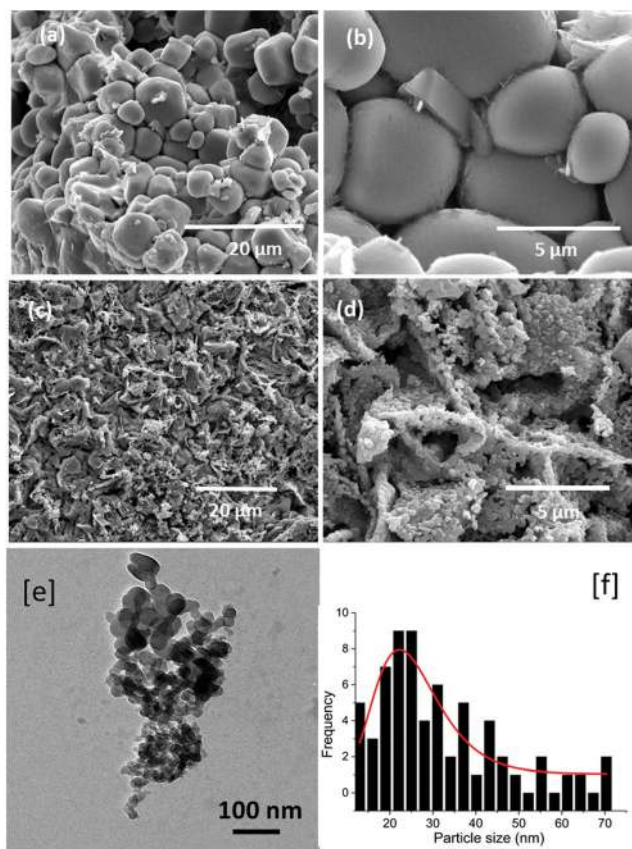


Fig. 4 (a) and (b) are SEM micrographs of Na-TMO, (c) and (d) show the SEM micrographs of ME-TMO and (e) shows the TEM micrograph of Na-TMO with the respective particle size distribution shown in (f).

sive spectroscopy (EDS), showed that both ME-TMO and Na-TMO had equimolar compositions (within  $\pm 3\%$  variation from the equimolar proportion and well-within the limits of experimental error) confirming the dissolution/accommodation of sodium and other cations in the rocksalt lattice. Atomic percentage of each element is listed in the Table S3.†

The soft agglomerates of the Na-TMO powder were dispersed by ultrasonication and studied using a TEM wherein the individual particles could be seen. The particle size distribution obtained from the TEM image is shown in Fig. 4. The mean particle size was found to be 32 nm with a standard deviation of 13 nm indicating a reasonably narrow distribution. The number density curve follows a Gaussian distribution.

It should be noted that the sizes obtained from SEM and TEM analysis refer to the particles which are composed of crystallites whose sizes were determined from the XRD patterns using the Scherrer formula. However, the fact that the average particle size obtained from TEM was close to the crystallite size in case of the Na-TMO indicated that the particles were either composed of a single crystal or had a very low degree of hard agglomeration.

#### 4.4 Bond analysis with FTIR

According to the group factor analysis theory, a rocksalt lattice with  $O_h^5$  symmetry has two  $F_{1U}$  IR active modes. The rocksalt

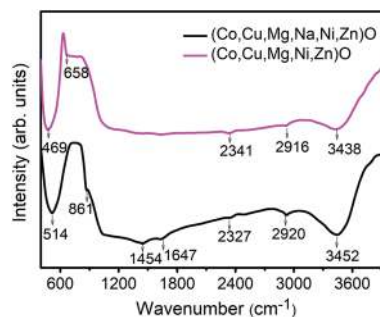


Fig. 5 FTIR spectra of Na-TMO and ME-TMO systems.

lattice has 4 equivalents points for the cation and the anion with each set of equivalents points giving rise to  $F_{1U}$  peaks, one being acoustic and the other optical.<sup>21</sup> The FTIR spectra of Na-TMO and ME-TMO are shown in Fig. 5. The observed broadening of the peaks at 469  $\text{cm}^{-1}$  and 514  $\text{cm}^{-1}$  for ME-TMO and Na-TMO respectively were attributed to the presence of different cations in the lattice as each would result in a different relaxation behaviour. When the structure symmetry is preserved, the peaks produced would be extremely close, but even a little shift would result in a broadened peak, as is observed when substitutional doping is done in the lattice. Pure  $\text{Na}_2\text{O}$  exhibits a peak at 1110  $\text{cm}^{-1}$  which was not observed in the FTIR spectra, hence ruling out the possibility of  $\text{Na}_2\text{O}$  being present as a minor second phase and confirming that the synthesised compound was phase-pure rocksalt.

The vibrations pertaining to the major constituents were further analysed. The transverse optical (T-O) frequency was used for calculating the force constant of the lattice using the relation eqn (1),

$$\omega = \frac{1}{2\pi c} \left( \frac{k}{\mu} \right)^{1/2} \quad (1)$$

where  $\omega$  is the wavenumber of the T-O vibration,  $k$  is the force constant and  $\mu$  was calculated from (eqn (2)), given as:

$$\mu = \frac{\sum (x \times M_C) \times M_O}{\sum (x \times M_C) + M_O} \quad (2)$$

where  $M_C$  is the atomic mass of each cation in the lattice,  $x$  is the mole fraction of the respective cation and  $M_O$  is the atomic mass of oxygen. The bond length,  $b$  was determined for each cation–oxygen bond from the force constant ( $k$ ) calculated for the respective cation, using (eqn (3)).<sup>22,23</sup>

$$b^3 = \frac{17}{k} \quad (3)$$

The obtained bond lengths from FTIR for Na-TMO and ME-TMO were 2.080 Å and 2.193 Å respectively. Table 2 lists the calculated force constants and the bond lengths which are in reasonable agreement with those determined from Rietveld refinement. It can also be seen that the bond length in case of the Na-TMO was less than that of ME-TMO due to the lower ionic radii of  $\text{Co}^{3+}$  and  $\text{Ni}^{3+}$  ions, resulting in the peak shift of

**Table 2** Force constant and bond length analysis from FTIR spectroscopy

Composition	Na-TMO	ME-TMO
Force constant ( $\text{N cm}^{-1}$ )	1.887	1.610
Bond length ( $\text{\AA}$ ) (from FTIR)	2.080	2.193
Bond length ( $\text{\AA}$ ) (from Rietveld)	2.118	2.119

the T-O vibration. The reduction in the intensity of the T-O mode and its broadening in the FT-IR spectrum of Na-TMO when compared to that of ME-TMO was attributed to the smaller crystallite size of the Na-TMO powders. Peaks at  $1650$  and  $3450\text{ cm}^{-1}$  in both the systems were attributed to the bending mode of water molecule.

#### 4.5 Structure distortion and defect analysis with Raman spectroscopy

Raman spectra of Na-TMO and ME-TMO are shown in Fig. 6. An ideal cubic rocksalt structure should not have any first order Raman active modes. The peaks at  $557\text{ cm}^{-1}$  in Na-TMO and at  $542\text{ cm}^{-1}$  in ME-TMO were asymmetric and could be deconvoluted into two peaks at  $470$  and  $550\text{ cm}^{-1}$  for Na-TMO and  $479$  and  $542\text{ cm}^{-1}$  for ME-TMO respectively. These two peaks were attributed to 1P TO and 1P LO modes respectively. 1P peaks are typically absent in a perfect cubic lattice due to the high symmetry, but the presence of a peak in the Raman spectra of the present two systems that could further be deconvoluted into the transverse optical and longitudinal optical peaks was a clear evidence of distortion in the cubic lattice. Since the vibration modes are related to the site symmetry of the lattice, substitution of different cations in the equivalent lattice point would lead to a lowering of the local translation symmetry. Apart from this, presence of defects and crystallite sizes being in the nano regime *etc.* would also cause the translation symmetry to be broken leading to the presence of 1P LO

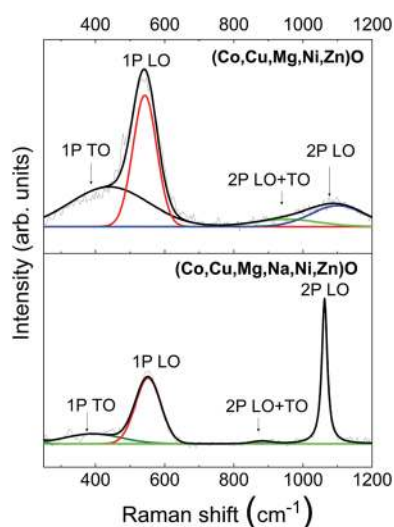
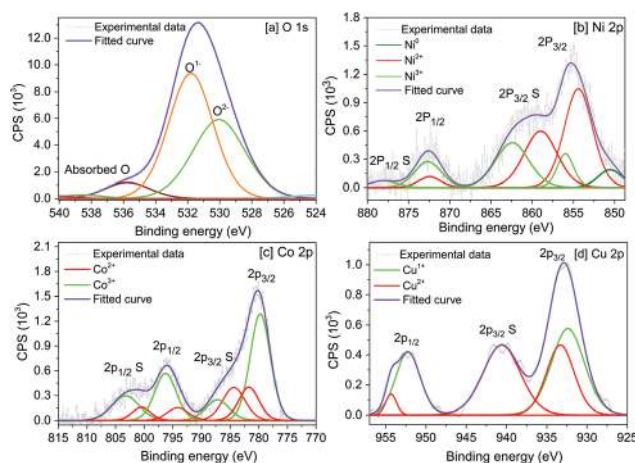
mode. Further, the lower intensity of the 1P LO mode was due to the Na-TMO having a smaller crystallite size. The peak at  $1090\text{ cm}^{-1}$  was attributed to the 2P LO peak of Na-TMO. The increase in the sharpness of the 2P LO peak can be attributed to the Frohlich interaction of 2P LO with the free carriers resulting in a resonated peak.<sup>24</sup> The defect concentration was further analysed by quantifying the phonon lifetime with the uncertainty equation (eqn (4)).

$$\tau = \frac{h}{\Delta E} \quad (4)$$

where  $\tau$  is the phonon lifetime,  $h$  is Planck's constant  $= 5.3 \times 10^{-12}\text{ cm}^{-1}\text{ s}$ , and  $\Delta E$  is FWHM of the 1 LO peak from the Raman spectra. In a defect-free crystal, the lattice oscillations are continuous and hence, the phonon lifetime will be longer compared to a crystal with defects. Lifetime of the LO mode was  $0.061\text{ ps}$  and  $0.065\text{ ps}$  for the Na-TMO and ME-TMO systems respectively. The shorter LO phonon lifetime of the Na-TMO system confirmed that it had a greater number of defect states compared to ME-TMO. The shorter LO phonon lifetime of the Na-TMO system was attributed to the combined effect of increased defect states and the presence of Na as an additional cation. The phonon lifetime also has a contribution from the anharmonicity of the crystal caused due to the phonon decay into other Brillouin zones and from entities breaking the translation symmetry such as point defects.<sup>25</sup>

#### 4.6 Oxidation states and defect analysis with X-ray photoelectron spectroscopy

The XPS survey spectrum and high resolution spectra of Na-TMO for cations with multiple oxidation states as well as oxygen are shown in Fig. 7. The main and satellite peaks of each of the oxidation states of every cation in the high resolution XPS (HR-XPS) scan was identified and the position of each peak is given in Table S4.† The assignment of the peaks to the various oxidation states for each cation was based on the binding energy values reported in literature and are given

**Fig. 6** Raman spectra of ME-TMO and Na-TMO powder.**Fig. 7** HR-XPS spectra of (a) O (b) Ni (c) Co and (d) Cu in the Na-TMO system.

**Table 3** Quantification of each ion at various oxidation states and the charge contribution

Element Oxidation state	Co		Cu		Mg +2	Ni			Zn +2	Na +1	O −2	Sum of the total charge
	+2	+3	+1	+2		0	+2	+3				
Cations (%)	1.41	4.51	2.98	1.46	6.68	0.94	3.93	0.80	5.82	7.19	35.30	
Normalized charge	2.82	13.54	2.98	2.92	13.36	0	7.85	2.40	11.65	7.19	−70.53	−5.83

in Tables S5–S11.† The percentages of the cations in each of the oxidation states are listed in Table 3. Defect concentration of the system was calculated from the XPS spectra by considering that electroneutrality of the structure had to be maintained. The charges on each cation was calculated by subtracting the percentage of covalency in each bond. O 1s peaks could be deconvoluted into three peaks (530.97 eV, 531.97 eV and 536.04 eV). The peak at 530.97 eV pertained to the lattice oxygen peak, arising from the ionic metal–oxygen bond. The high binding energy peak at 531.97 eV arose from oxygen with the lesser co-ordination number, while the peak at 536.08 eV was due to OH bond resulting from adsorbed moisture in the material. The percentage of covalency in the oxygen bond was estimated from the O 1s peaks using the method given by Wu *et al.*<sup>26</sup> Covalency percentage of each cation was calculated from the satellite peak, as satellite peaks are produced due to the final state effect and sensitive to the bond with oxygen, using the relation (eqn (5)).

$$\text{Covalency \%} = \frac{I_s - S}{2} \quad (5)$$

where  $I_s$  is the intensity ratio of the satellite peak to the main peak, and  $n$  and  $S$  are constants whose values were taken from literature.<sup>27</sup> For the cations which do not have a satellite peak, the percentage of covalent bonding was taken from reports of studies on the individual (unary) oxides.<sup>28</sup> The covalent percentage of the bond was eliminated while calculating the defect concentration, as it does not contribute to the off-stoichiometry in the lattice. From Table 3 it can be seen that if all the positive charge units can be summed up by considering the oxidation states of the all the cations and their corresponding percentage, a total of 64.70 positive charge units can be arrived at and 70.53 units of negative charge was present in the ionic oxygen bond of the Na-TMO lattice and so, in order to ensure charge neutrality the excess negative charge of 5.83 would be compensated by the creation of 2.91% oxygen vacancies in the lattice. This figure also agreed well with the quantification obtained from Rietveld analysis. A small fraction of Ni was found to be in the metallic (0 oxidation) state, attributed to the presence of oxygen vacancies in the surrounding and were bonded to the lattice by sharing degenerate electrons.

The formation of metallic Ni has been reported from theoretical studies by modelling clusters of NiO as well as by doping with lower oxidation state cations.<sup>29,30</sup> From the XPS spectra, it can be seen that 10.17% out the maximum 50% cations were in the +1 oxidation state ( $\text{Na}^{1+}$  and  $\text{Cu}^{1+}$ ). This

could be charge compensated for electrical neutrality either by oxygen vacancies or by some cations (specifically Ni and Co) taking higher oxidation states. From the estimated value of 2.91% oxygen vacancies, it is clear that oxygen vacancies alone were not sufficient and so, cations like Ni and Co had to take higher oxidation states. By quantification from the HR-XPS spectrum for Ni it can be seen that the higher oxidation states of Ni could compensate for only 0.80% and the balance 3.55% could be offset only by Co taking up higher oxidation states. Therefore, to maintain charge neutrality in the lattice, the presence of Co became essential. This was experimentally confirmed from the fact that the (Cu,Na,Ni,Mg,Zn)O system was not phase-pure and had minor amount of secondary phases, further explained in section 4.9.

#### 4.7 Effect of oxygen vacancies on the lattice parameter

The lattice parameter of Na-TMO obtained from Rietveld refinement (while considering the structure to be cubic, shown in Table 1) was found to be less than that of the “parent” ME-TMO. On the other hand, according to Vegard’s law,<sup>31</sup> it is expected that the lattice parameter would increase in the presence of Na due to its larger ionic radius (102 pm). In the case of sodium doping in NiO, not much change in the lattice parameter has been reported, although there should have been an increase due to the presence of Na.<sup>8</sup> One factor for lattice contraction in Na-TMO could be due to the creation of oxygen vacancies that are needed to maintain charge neutrality when Na is doped in the system, resulting in a decrease in the lattice parameter of the system. Park *et al.*<sup>32</sup> have shown through DFT calculations that when an oxygen vacancy forms in the NiO lattice, the Ni atoms relax inwards reducing the lattice parameter. Similar observation of lattice contraction due to oxygen vacancy formation has been observed in ZnO also.<sup>33</sup> A lattice contraction could, therefore, imply the presence of oxygen vacancies in the lattice. Further, Rietveld analysis showed that there was 6.8% oxygen vacancy present in the anion lattice, which was also supported from the XPS results shown in section 4.6 and that indicated the presence of 5.83% oxygen vacancy (out of 100). A second reason for lattice contraction could be due to Co (or Ni) taking a higher oxidation state in order to maintain charge neutrality in the structure. The ionic radii of both cobalt and nickel in the +3 oxidation states with high spin having a 6-fold co-ordination number is lesser than the respective ionic radii of Co and Ni in the +2 oxidation states. The presence of oxygen vacancies as well as Ni and Co cations in higher oxidation states was evident from XPS studies (as seen in section 4.6). The additive effect of



these two factors would have caused the lattice parameter to decrease.

Change in the oxidation states of cobalt and nickel and the formation of oxygen vacancies was further confirmed from magnetic characterization studies. Magnetic susceptibility of the system, calculated from the slope of the  $M-H$  curves (Fig. 2) at high field, revealed that Na-TMO had a higher susceptibility value compared to ME-TMO. As  $\text{Na}_2\text{O}$  is only a diamagnetic constituent,<sup>34</sup> the increase in the magnetic moment could not result directly from the presence of the Na ion. However, due to the presence of the Na ion in the lattice, creation of oxygen vacancies and formation of  $\text{Co}^{3+}$  and  $\text{Ni}^{3+}$  have taken place. Both  $\text{Co}^{3+}$  and  $\text{Ni}^{3+}$  have higher magnetic moments in the high spin state, which has resulted in an increase in the overall magnetic moment of the Na-TMO. Further, due to the oxygen vacancies, the formation of a bound magnetic polaron (BMP) would be possible leading to a ferromagnetic or antiferromagnetic interaction in the presence of localised carriers, thereby increasing the magnetic susceptibility. Hence, the  $M-H$  characteristics of the Na-TMO clearly provide the proof that oxygen vacancies as well as  $\text{Co}^{3+}$  and  $\text{Ni}^{3+}$  had formed due to the presence of Na in the distorted rocksalt lattice of the “parent” ME-TMO.

#### 4.8 Effect of ionic radii in phase formation

Ionic radii of the constituent cations in the various possible oxidation states, coordination number and the percentage ionic radii difference from the (reference) smallest cation ( $\text{Ni}^{2+}$ ) are listed in Table S12.† Sodium ion has the largest radii with a size difference of 47.8% compared to the smallest  $\text{Ni}^{2+}$  ion in the synthesized system. Till date, the selection of cations in multicomponent oxides has been based predominantly on the assumption that the cations should have nearby ionic radii (limited to a difference of about 15% as given by the Hume-Rothery/Pauling's rule for single-phase formation). However, the fact that Na could still form a single-phase in the present Na-TMO system despite the large size difference clearly showed that in this particular case Hume Rothery/Pauling's rule is not an essential criterion. It is noteworthy that the ratio of cation radius ( $R_c$ ) to anion radius ( $R_a$ ) allows a sodium ion to be in an octahedral coordination within the  $f\bar{m}3m$  space group of the stable structure of sodium oxide and hence, the present structure could accommodate the sodium ions with slight distortion in the lattice. The ideal intensity ratio of the (200):(111) XRD peaks is 1.66. However, the ME-TMO by itself deviated from this ratio and had a value of 1.57 which Bérardan *et al.*<sup>35</sup> had attributed to the Jahn-Teller effect due to the presence of the copper in the lattice. This structure is not very different from the Na-TMO rocksalt lattice in terms of symmetry. The Na-TMO, on the other hand, had a ratio of 1.83 showing a much higher deviation, implying that substitution by sodium atoms had taken place in the lattice with some further distortion.

To determine the upper limit of the ionic radii which can be dissolved into the ME-TMO lattice, potassium ions which are nearly twice as large as  $\text{Ni}^{2+}$  ions, were added in equimolar

proportion to the ME-TMO system (K-TMO). This resulted in the formation of the rocksalt phase along with secondary phases such as copper oxide as well as metallic nickel and copper. Clearly, there appears to be a limitation in the ionic radii up to which a substitution in the lattice is possible. It is interesting to note the formation of Ni and Cu, which was possibly due to the reduction of NiO and CuO by potassium. As  $\text{K}_2\text{O}$  decomposes at 800 °C and the calcination was carried out at 1000 °C, there was no residual potassium oxide present. In a separate experiment, calcium which has a slightly smaller ionic radius (1.0 Å) compared to sodium ion (1.02 Å) but is 44.9% larger compared to the smallest ion in the lattice ( $\text{Ni}^{2+}$ ), was added to the “parent” ME-TMO system (Ca-TMO) to check the solubility. Rietveld refinement of Ca-TMO is shown in the Fig. S1.† It was observed that Ca dissolved partially into the lattice which was evident from the increased lattice parameter of Ca-TMO but 7.72% CaO formed as a second phase. Hence, it is evident that although Na-TMO exhibited a single phase, it is not enough that the addition of a cation with ionic radii less than that of Na would result in a single phase formation, even though Ca has the same oxidation state (+2) as the stable form of the other transition metal cations.

This further indicated that if a cation with significantly higher ionic radii compared to the other transition metal cations in the ME-TMO lattice has to be incorporated in equimolar proportion to form a single phase, it should be able to induce non-stoichiometry in the lattice, which would allow the accommodation of the larger ion in the lattice. Fig. 8 shows the X-ray diffraction patterns of K-TMO and Ca-TMO.

#### 4.9 Effect of oxidation state and individual cations on phase formation

To further analyse the factors enabling the accommodation of sodium in the parent ME-TMO rocksalt structure, five component systems with one transition metal element being systematically removed were synthesised under the same conditions as the (Co,Cu,Mg,Na,Ni,Zn)O system. XRD patterns of the synthesised systems are shown in Fig. 9. Removing one of the cations such as Ni, Mg, Cu or Zn did not affect the solid solution formation and the structure remained phase-pure rocksalt. Only on the extraction of cobalt, minor secondary

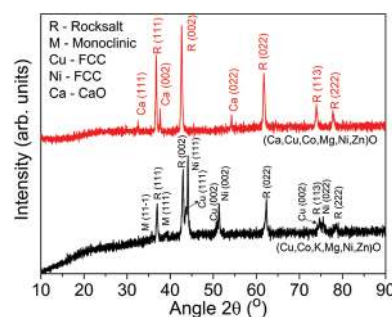


Fig. 8 X-ray diffraction patterns of K-TMO and Ca-TMO exhibiting second phase formation.

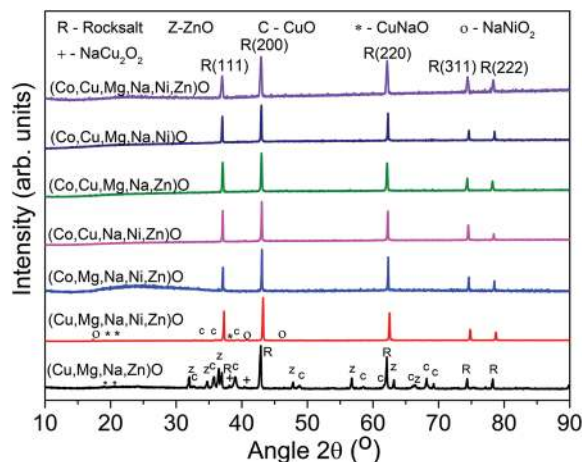


Fig. 9 X-ray diffraction patterns of Na-TMO compositions with lower order combinations by systematically extracting one or more of the transition metal cations.

phases were produced in the (Cu,Mg,Na,Ni,Zn)O system with the major phase still being rocksalt. From this, it is evident that cobalt is an essential candidate for single-phase formation by maintaining the charge neutrality and hence, the structural stability of the lattice. However, as the major phase formed was still rocksalt and as the relative proportions of the secondary phases were very low, it was assumed that Ni also favoured sodium dissolution into the lattice although not as effectively as Co. To further confirm this hypothesis, a four-component system was synthesised without Ni and Co and it was seen that the secondary-phase fractions increased substantially. The major phases formed were rocksalt – 52%, monoclinic – 26%, hexagonal – 20.17% with some minor amounts of  $\text{Na}_2\text{Cu}_2\text{O}_2$  prototype (Orthorhombic) and  $\text{NaCuO}$  prototype (tetragonal) phases. Rietveld refinement of the X-ray diffraction pattern is shown in Fig. S2.† Hence it is clear, Ni and Co played major roles in forming a single-phase structure.

It is noteworthy that the major elements of the ME-TMO system such as Ni and Co tend to take higher oxidation states in their intrinsic unary oxides. Therefore, it could be speculated that the ME-TMO would also have metal cations in higher oxidation states and to compensate for that, some metal vacancies would be present. As seen from the XPS studies, due to the presence of cations in the +3 oxidation states, incorporation of +1 oxidation elements was possible in the ME-TMO system. This is also supported by the fact that Li could be accommodated in the ME-TMO lattice up to equimolar percentage and K up to 5%.<sup>11</sup> However, when Cr, Mn and Fe (all of which exhibit stable +3 oxidation states) were, in turn, added to the ME-TMO system in equimolar proportion, it was found that the ME-TMO lattice was unable to accommodate the +3 oxidation state elements (Cr, Mn or Fe), as it would require either the formation of additional metal vacancies or the cations would have to take lower oxidation states. As the ME-TMO lattice already has metal vacancies due to the presence of Co and Ni in higher oxidation states, the generation of

additional metal vacancies to maintain charge neutrality would become extremely difficult and the formation of secondary phases would take place. The XRD patterns of the parent ME-TMO with Cr, Mn and Fe individually added (shown in Fig. 10) revealed the presence of second phases. It is worth pointing out in this context that Bérardan *et al.*<sup>36</sup> had reported that addition of +3 elements such as Ga resulted in multiple phase formation.

This conclusively showed that the ME-TMO systems have metal cations in higher oxidation states enabling the accommodation of cations with +1 oxidation state and thus, maintain charge neutrality. No such possibility existed for the accommodation of cations with +3 oxidation states as the creation of more metal vacancies in the single-phase structure was not energetically favoured.

#### 4.10 Effect of high entropy

Rost *et al.*<sup>2</sup> have clearly established that the ME-TMO is an entropy stabilised oxide as the Gibbs free energy,  $\Delta G = \Delta H_{\text{mix}} - T\Delta S_{\text{mix}}$  would be negative since the  $\Delta S_{\text{mix}}$  component, which arose from the configurational entropy of the system was large due to the presence of a multiple number of cations in equimolar proportion. The configuration entropy, given by  $S_{\text{config}} = -R \left( \sum_{i=1}^n (x_i \ln x_i) \right)$  was 1.61R for the 5 component system and sufficient to offset the enthalpy penalty. Addition of a 6th component would have increased the configurational entropy to 1.79R, thereby further aiding the stabilisation of the single phase, provided no formation of microstates or ordering of any kind took place (which would decrease the  $\Delta S_{\text{mix}}$  of the system) and issues of creating more defect states to accommodate larger-sized or aliovalent cations or generating vacancies in order to maintain electroneutrality of the structure remained energetically favourable. This was the reason why addition of Fe, Mn, Cr, Ca or K at equimolar proportions did not lead to stabilisation of the rocksalt phase despite the increase in configurational entropy. On the other hand, the addition of Na did not pose these problems and hence, the

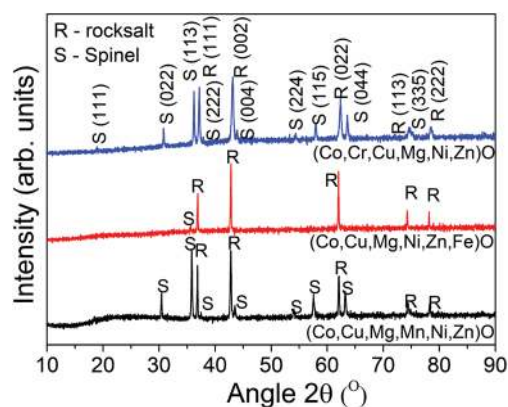


Fig. 10 X-ray diffraction patterns of the ME-TMO system with systematic additions of +3 oxidation state cations.



stable phase-pure rocksalt structure was maintained. Further, Sarkar *et al.*<sup>37</sup> have reported that the ME-TMO derivatives with small additions of Na, K, Li *etc.* are entropy stabilised systems with a phase-pure rocksalt structure, showing phase reversion during cyclic heat treatment. Therefore, it can be conclusively stated that the present Na-TMO system is a high entropy oxide.

## 5 Conclusions

A single-phase, multicomponent, equimolar oxide system with 5 transition metal cations and one alkali cation, (Co,Cu,Mg,Na,Ni,Zn)O called Na-TMO, having a phase-pure rocksalt structure was successfully synthesised and characterised. For the sake of comparison a multicomponent equimolar transition metal oxide, ME-TMO (Co,Cu,Mg,Ni,Zn)O, was also synthesised. Systematic extraction of a transition metal cation from the Na-TMO revealed the importance of maintaining electroneutrality in the structure for the formation of a single phase and implied the need for multivalent cations in order to enable the system to accommodate cations of varied ionic radii. Infra-red spectroscopy, Raman spectroscopy, vibrating sample magnetometry and X-ray photoemission spectroscopy confirmed that accommodation of sodium in the rocksalt lattice was possible through the formation of defect states and by the conversion of cobalt and nickel to higher oxidation states. Second phase formation on Ca addition showed that the presence of non-stoichiometry was essential to accommodate large-sized cations and form a phase-pure structure. Incorporation of cations with stable +3 oxidation states (Cr, Fe or Mn) in equimolar proportions to form a phase-pure rocksalt structure was not possible due to unfavourable energetics. Thus, it was concluded that the Hume-Rothery/Pauling's rules regarding size limitation and same oxidation states of the cations were not necessarily essential criteria for the formation of a phase-pure crystal structure.

## Conflicts of interest

There are no conflicts of interest to declare.

## Acknowledgements

We acknowledge the DST, GoI for funding the NFMTC where this work was carried out and SAIF IIT Madras for the FTIR and VSM facilities, and Nanotechnology lab, IIT Madras for the XRD measurements. The support from a DST, SERB project SERB/F/4352/2017-2018 is gratefully acknowledged.

## References

- 1 B. Murty, J. Yeh and S. Ranganathan, *High Entropy Alloys*, Butterworth-Heinemann, Boston, 2014, pp. 1–218.
- 2 C. M. Rost, E. Sachet, T. Borman, A. Moballeghe, E. C. Dickey, D. Hou, J. L. Jones, S. Curtarolo and J.-P. Maria, *Nat. Commun.*, 2015, **6**, 8485.
- 3 A. Sarkar, C. Loho, L. Velasco, T. Thomas, S. S. Bhattacharya, H. Hahn and R. Djenadic, *Dalton Trans.*, 2017, **46**, 12167–12176.
- 4 K. Chen, X. Pei, L. Tang, H. Cheng, Z. Li, C. Li, X. Zhang and L. An, *J. Eur. Ceram. Soc.*, 2018, **38**, 4161–4164.
- 5 A. Sarkar, R. Djenadic, D. Wang, C. Hein, R. Kautenburger, O. Clemens and H. Hahn, *J. Eur. Ceram. Soc.*, 2018, **38**, 2318–2327.
- 6 S. Jiang, T. Hu, J. Gild, N. Zhou, J. Nie, M. Qin, T. Harrington, K. Vecchio and J. Luo, *Scr. Mater.*, 2018, **142**, 116–120.
- 7 J. Da, M. Stygar, A. Mikula, A. Knapik, K. Mroczka, W. Tejchman, M. Danielewski and M. Martin, *Mater. Lett.*, 2018, **216**, 32–36.
- 8 S. Yang, J. Kim, S. Song, D. Lee, T.-S. Ju, J.-S. Bae and S. Park, *Ceram. Int.*, 2017, **43**, 11898–11901.
- 9 C. Chen, F. Delorme, F. Schoenestein, M. Zaghrioui, D. Flahaut, J. Allouche and F. Giovannelli, *J. Eur. Ceram. Soc.*, 2019, **39**, 346–351.
- 10 M. H. Han, E. Gonzalo, G. Singh and T. Rojo, *Energy Environ. Sci.*, 2015, **8**, 81–102.
- 11 N. D. Bérardan, S. Franger and A. K. Meena, *J. Mater. Chem. A*, 2016, **4**, 9536–9541.
- 12 H. Kim, H. Kim, Z. Ding, M. H. Lee, K. Lim, G. Yoon and K. Kang, *Adv. Energy Mater.*, 2016, **6**, 1600943.
- 13 H. L. Tuller, *Solid State Ionics*, 2000, **131**, 143–157.
- 14 A. M. Abdalla, S. Hossain, A. T. Azad and P. M. I. Petra, *Renewable Sustainable Energy Rev.*, 2018, **82**, 353–368.
- 15 A. Sarkar, R. Djenadic, N. J. Usharani, K. P. Sanghvi, V. S. K. Chakravadhanula, A. S. Gandhi, H. Hahn and S. S. Bhattacharya, *J. Eur. Ceram. Soc.*, 2017, **37**, 747–754.
- 16 N. Qiu, H. Chen, Z. Yang, S. Sun, Y. Wang and Y. Cui, *J. Alloys Compd.*, 2019, **777**, 767–774.
- 17 J. S. Smart and S. Greenwald, *Phys. Rev.*, 1951, **82**, 113–114.
- 18 C.-G. Stefanita, *Magnetism*, Springer-Verlag Berlin Heidelberg, 1st edn, 2012.
- 19 S. Roy, A. G. Joshi, S. Chatterjee and A. K. Ghosh, *Nanoscale*, 2018, **10**, 10664–10682.
- 20 S. C. Erwin, L. Zu, M. I. Haftel, A. L. Efros, T. A. Kennedy and D. J. Norris, *Nature*, 2005, **436**, 91.
- 21 D. L. Rousseau, R. P. Bauman and S. P. S. Porto, *J. Raman Spectrosc.*, 2018, **10**, 253–290.
- 22 H. Singh and K. L. Yadav, *Ceram. Int.*, 2015, **41**, 9285–9295.
- 23 N. J. Usharani and S. Bhattacharya, *Ceram. Int.*, 2020, **46**, 5671–5680.
- 24 S. J. Chen, H. Y. Xu, S. X. Wang and K. Suzuki, *Integr. Ferroelectr.*, 2013, **144**, 1–8.
- 25 L. Bergman, D. Alexson, P. L. Murphy, R. J. Nemanich, M. Dutta, M. Strosio, C. Balkas, H. Shin and R. F. Davis, *Phys. Rev. B: Condens. Matter Mater. Phys.*, 1999, **59**, 977–982.

- 26 L. Q. Wu, Y. C. Li, S. Q. Li, Z. Z. Li, G. D. Tang, W. H. Qi, L. C. Xue, X. S. Ge and L. L. Ding, *AIP Adv.*, 2015, **5**, 097210.
- 27 S. Asada and S. Sugano, *J. Phys. Soc. Jpn.*, 1976, **41**, 1291–1299.
- 28 L. Pauling, *The Nature of the Chemical Bond and the Structure of Molecules and Crystals: An introduction to modern structural chemistry*, Cornell University Press, New York, 3rd edn, 1960, p. 93.
- 29 L. G. M. Pettersson and G. Pacchioni, *Chem. Phys. Lett.*, 1994, **219**, 107–112.
- 30 Y. Rama, K. Lee, C. Park, S. Kun, H. Jae, D.-S. Yang and S. Seo, *Thin Solid Films*, 2015, **591**, 255–260.
- 31 A. R. Denton and N. W. Ashcroft, *Phys. Rev. A*, 1991, **43**, 3161–3164.
- 32 S. Park, H.-S. Ahn, C.-K. Lee, H. Kim, H. Jin, H.-S. Lee, S. Seo, J. Yu and S. Han, *Phys. Rev. B: Condens. Matter Mater. Phys.*, 2008, **77**, 134103.
- 33 X. Li, Y. Wang, W. Liu, G. Jiang and C. Zhu, *Mater. Lett.*, 2012, **85**, 25–28.
- 34 K. Savithri and S. Ramachandra Rao, *Proc. – Indian Acad. Sci., Sect. A*, 1942, **16**, 221–230.
- 35 D. Bérardan and C. Herrero, *J. Alloys Compd.*, 2017, **704**, 693–700.
- 36 D. Bérardan, S. Franger, D. Dragoe, A. K. Meena and N. Dragoe, *Phys. Status Solidi RRL*, 2016, **10**, 328–333.
- 37 A. Sarkar, Q. Wang, A. Schiele, M. R. Chellali, S. S. Bhattacharya, D. Wang, T. Brezesinski, H. Hahn, L. Velasco and B. Breitung, *Adv. Mater.*, 2019, **31**, 1806236.